Random network peristalsis in *Physarum polycephalum* organizes fluid flows across an individual

Karen Alim[a,1,2], Gabriel Amselem[a,b,1], François Peaudecerf[a], Michael P. Brenner[a], and Anne Pringle[b]

[a]School of Engineering and Applied Sciences and Kavli Institute for Bionano Science and Technology, and [b]Department of Organismic and Evolutionary Biology, Harvard University, Cambridge, MA 02138

Edited by Charles S. Peskin, New York University, New York, NY, and approved July 1, 2013 (received for review March 19, 2013)

Individuals can function as integrated organisms only when information and resources are shared across a body. Signals and substrates are commonly moved using fluids, often channeled through a network of tubes. Peristalsis is one mechanism for fluid transport and is caused by a wave of cross-sectional contractions along a tube. We extend the concept of peristalsis from the canonical case of one tube to a random network. Transport is maximized within the network when the wavelength of the peristaltic wave is of the order of the size of the network. The slime mold *Physarum polycephalum* grows as a random network of tubes, and our experiments confirm peristalsis is used by the slime mold to drive internal cytoplasmic flows. Comparisons of theoretically generated contraction patterns with the patterns exhibited by individuals of *P. polycephalum* demonstrate that individuals maximize internal flows by adapting patterns of contraction to size, thus optimizing transport throughout an organism. This control of fluid flow may be the key to coordinating growth and behavior, including the dynamic changes in network architecture seen over time in an individual.

acellular | fungi | myxomycete

Many organisms, including diverse species of slime molds and fungi, grow and forage as remarkably large networks. Networks explore the environment to locate scarce and spatially disjunct resources (1). The mechanisms used by an individual to integrate disparate sources of information, coordinate growth, and thrive across heterogeneous habitats remain unknown. Foragers adapt body morphologies around newly discovered materials, but have no nervous system, and are a stark contrast to animals, where an evolved neural circuitry coordinates complex behaviors. In slime molds and fungi, the internal flows within a tubular network may be critical to the coordination of growth across an individual.

The slime mold *Physarum polycephalum* grows as a single complex of tubes and has emerged as a focus of research on network behaviors. The morphological dynamics of *P. polycephalum* are repeatedly characterized as "intelligent" (2–6). For example, *P. polycephalum* can connect two food sources, using the shortest path in a maze (4), and networks connecting multiple food sources find a good compromise between efficiency, reliability, and cost, comparable to optimized, man-made, transport networks (5). Optimization is also a target of parallel research exploring theoretical models of transport networks (7–9). The mechanisms enabling the growth and coordination of *P. polycephalum*'s networks are unknown.

Networks of *P. polycephalum* possess a characteristic, periodic cytoplasmic streaming ("shuttle streaming"); the streaming extends across an individual (10). The network consists of tubes made of a gel-like outer layer enclosing the cytoplasmic fluid, and the fluid oscillates forth and back across a network with a period of about 100 s (11). The most natural hypothesis to explain flow suggests it is caused by observed cross-sectional contractions of the tubes generated by the actin cytoskeleton in the outer gel layer (12). Contraction-driven flow is a ubiquitous mechanism causing biological transport, particularly in the form of peristalsis, which propagates contents within the human digestive tract and other tubular, linear organs (13). At the heart of the peristaltic mechanism is a spatial correlation of the phases of contractions, so that the phase increases linearly with distance along the tube. This phase pattern causes an oscillatory flow and moves material along a tube (14). Peristalsis has often been hypothesized as a transport mechanism in *P. polycephalum* (15, 16) and inspired flow calculations in small single-veined individuals (17); because an organism has a finite size, transport would be caused primarily by oscillatory flow and not net flux. The existence of a peristaltic mechanism within the slime mold is supported by observations of phase waves of contractions (18–21). However, to the best of our knowledge, all attempts to correlate contractions with cytoplasmic flow have failed, and some experiments even appear to contradict the existence of peristalsis in *P. polycephalum* (22–25).

To explore the organization of flows within *P. polycephalum* we investigated individuals growing without food sources, when the slime molds are actively foraging and the tubes form a closed, essentially random network (Fig. 1). We first investigated the cause of flows by measuring the spatiotemporal development of cross-sectional contractions and cytoplasmic flow and developed a theoretical description of contraction-driven flow. Using the data and model we demonstrate that the cytoplasmic flows are in fact caused by cross-sectional contractions present throughout the organism. We next investigated the coordination of flows by monitoring the phases of contractions, which were defined locally as the fraction of the contraction cycle elapsed relative to the last maximum (Fig. 1*A*). We tracked the phases of contractions at each point in time across entire individuals and generated maps of the phase dynamics across whole organisms. We observe an almost linear gradient of phases, with wavelength scaling with organism size. We derived a theoretical generalization of the concept of peristalsis to a network of tubes. This framework shows that even in a complex network, an almost linear phase gradient of a single phase cycle is optimal for maximizing transport. In fact, theoretical phase patterns derived from this framework across *P. polycephalum* network architectures, mapped from real individuals, agree with experimentally observed phase patterns. Thus, flows in *P. polycephalum* are driven by peristalsis and optimized for transport across the entire organism. The lack of any local correlation between cross-sectional contractions and flow (22–25) is specifically caused by the propagation of peristaltic flows generated throughout the network and the complexity of the network architecture. The slime mold *P. polycephalum* appears to coordinate foraging behavior

Author contributions: K.A., G.A., F.P., M.P.B., and A.P. designed research, performed research, and wrote the paper.

The authors declare no conflict of interest.

This article is a PNAS Direct Submission.

[1]K.A. and G.A. contributed equally to this work.

[2]To whom correspondence should be addressed. E-mail: kalim@seas.harvard.edu.

This article contains supporting information online at www.pnas.org/lookup/suppl/doi:10.1073/pnas.1305049110/-/DCSupplemental.

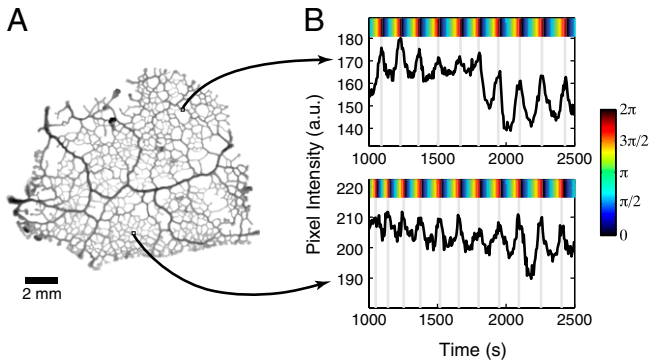

Fig. 1. (*A*) Bright-field image of *P. polycephalum*, a true slime mold (myxomycete) that grows as a network of tubes. (*B*) Transmitted light intensity at two sample tubes as a function of time. Vertical lines indicate maxima of oscillations. The oscillating cross-sectional contractions of a tube directly modulate the intensity of transmitted light (Fig. S1), enabling the contraction state and the phase of contractions over time to be identified and tracked. Phase as a function of time is shown at the top of each graph, using a periodic color code that cycles from black at zero to blue, green, and red and then back to black at 2π.

by optimizing transport within its network of tubes, enabling resources to be distributed across an entire individual.

Results

Cross-Sectional Contractions of Tubes Drive Flows in *P. polycephalum*. We let *P. polycephalum* endocytose fluorescent beads of 1 μm in diameter and recorded time series of the flowing beads along a single tube of a network over 30–60 min, using fluorescent imaging. Simultaneously, the slime mold was illuminated from below and imaged using bright-field microscopy, at a frame rate of 10 images per minute and magnifications ranging from 1× to 5× (*Materials and Methods*). An overlay of the bright-field and fluorescent images can be seen in Fig. 2*A*, where the bead positions at two consecutive time points are shown in red and green, respectively. The radii of tubes were determined from the bright-field images, and their spatiotemporal development served as the sole input to our model of flows within a contracting tube (Fig. 2*B*).

To explore flows driven by cross-sectional contractions of tubes, we solve the equations for incompressible fluid flow. If $a=a(z,t)$ is the radius of a tube as a function of its axial coordinate z and time t, the flow velocities u and v along and perpendicular to the tube follow from solving the Stokes equations

$$\mu\nabla^2\vec{u}=\nabla P,\quad \text{with } \vec{u}=(u,v), \qquad [1]$$

combined with the no-slip boundary conditions on the walls, $u=0$ and $v=\frac{\partial a}{\partial t}$ at $r=a$. The Stokes equations are a good approximation for the flows created by *P. polycephalum*: Using a representative tube radius of $a_0=50$ μm, a velocity of $u=1$ mm/s, and the kinematic viscosity of water, the Reynolds number is small, $Re=2ua_0/\nu\sim 0.1$. Moreover, the tube radius a_0 is much smaller than the oscillatory boundary layer thickness $\sqrt{\nu/\omega}$, with $\omega=0.05$ Hz. Our experiments show that the characteristic length scale of the contraction is much larger than the radius of the tube, which suggests a generalization of the ansatz of refs. 14, 26, and 27,

$$u(z,r,t)=2\overline{u}(z,t)\left(1-\left(\frac{r}{a(z,t)}\right)^2\right), \qquad [2]$$

$$v(z,r,t)=\frac{\partial a(z,t)}{\partial t}\left(\frac{r}{a(z,t)}\right)\left(2-\left(\frac{r}{a(z,t)}\right)^2\right)+2\frac{\partial a(z,t)}{\partial z}\overline{u}(z,t)\left(\frac{r}{a(z,t)}\right)\left(1-\left(\frac{r}{a(z,t)}\right)^2\right), \qquad [3]$$

which satisfies the no-slip boundary condition at $r=a$. Imposing $\nabla\vec{u}=0$ implies a relationship between the cross-sectionally averaged axial flow velocity $\overline{u}$ and the contractions $\frac{\partial a}{\partial t}$,

$$\overline{u}(z,t)=\frac{\overline{u}(z_0,t)a(z_0,t)^2}{a(z,t)^2}-\frac{2}{a(z,t)^2}\int_{z_0}^{z}d\tilde{z}\,a(\tilde{z},t)\frac{\partial a(\tilde{z},t)}{\partial t} \qquad [4]$$

$$\overline{Q}(z,t)=\overline{Q}(z_0,t)-2\pi\int_{z_0}^{z}d\tilde{z}\,a(\tilde{z},t)\,\frac{\partial a(\tilde{z},t)}{\partial t}, \qquad [5]$$

where the cross-sectionally averaged fluid flux is $\overline{Q}=\pi a^2\overline{u}$. In Eq. **5**, the first term describes the flow input to a particular tube from other tubes at $z=z_0$, whereas the second term is the flow generated by the contractions in the tube over the length $z-z_0$, ΔQ.

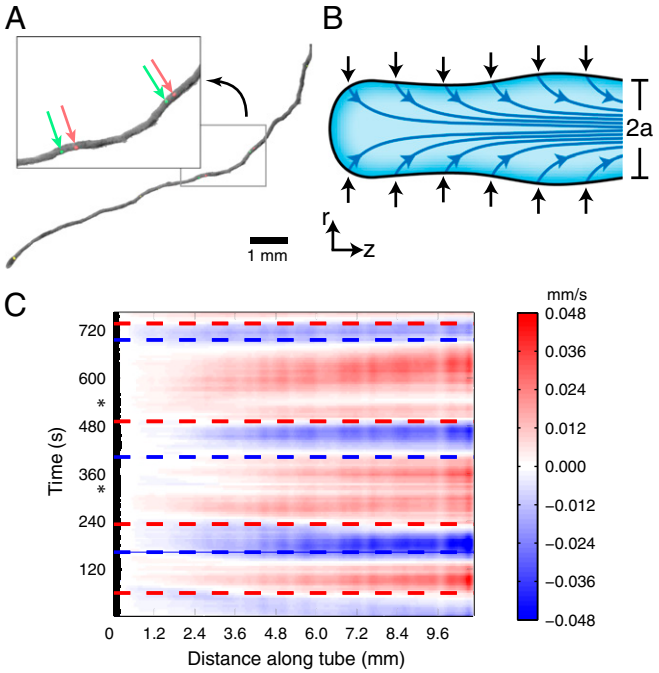

Fig. 2. Testing for a causal relationship between cross-sectional tube contractions and cytoplasmic flows. (*A*) Overlay of bright-field (gray) and fluorescent (red and green) images, to simultaneously measure tube radius along a tube over time and track fluorescent beads advected by the flow. Moving beads, indicated by arrows, are red in an initial time frame and green in the time frame taken 1 s later. (*B*) Illustration of how cross-sectional contractions (black arrows) of a tube of radius *a* drive fluid flow (blue streamlines) along a 3D tube extending in radial *r* and longitudinal *z* dimensions. (*C*) Flows predicted by the contracting tube model based on experimentally obtained tube radii. Flow to the right, away from the tube end (0 mm), is shown in red and that toward the tube end is in blue, highlighting flow arrests (marked by asterisks) and reversals in white. Overlaid experimental time points of real flow reversals (dashed lines) show very good agreement with the model. Moreover, time points where the model predicts that the flow arrests without reversing its direction (asterisks) correspond to what is observed experimentally (Movie S1).

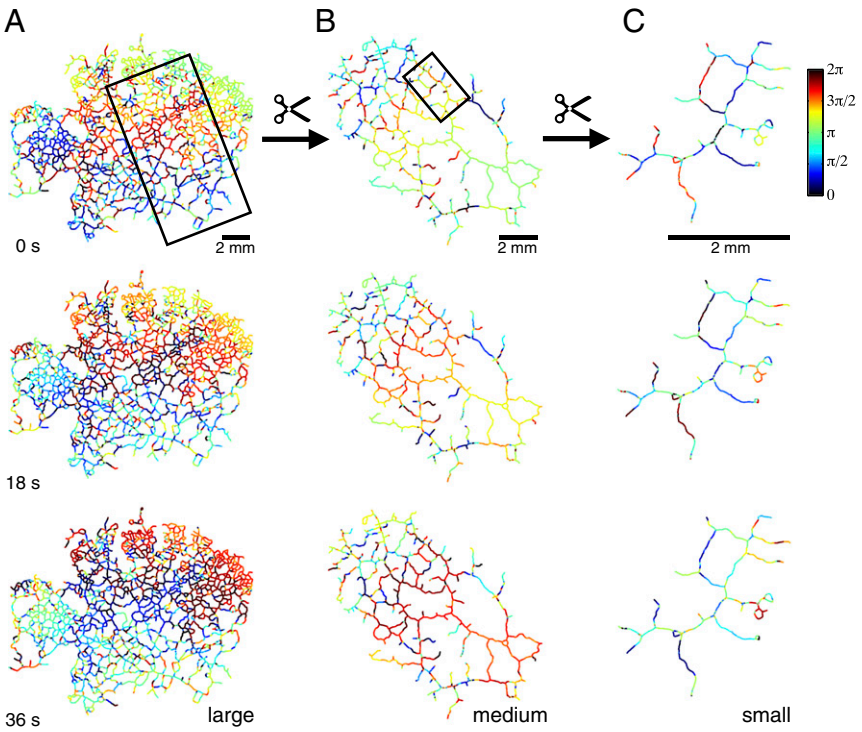

Fig. 3. (*A*–*C*) Typical phase patterns of *P. polycephalum* networks ranging from approximately (*A*) 17 mm to (*C*) 3 mm. Independently of size, an almost linear phase gradient establishes across the network. The gradient encompasses a single cycle of zero to 2π extending along the longest axis of an individual. Colors mark the phases of contractions calculated as the fraction of the contraction cycle elapsed relative to the last maximum (Fig. 1*B*). (*A* and *B*, *Top*) Black rectangles mark the approximate regions cut at the end of each experiment to obtain the medium network (*B*) from the large network (*A*) and the small network (*C*) from the medium network (*B*), respectively. For tube architecture see bright-field data in Fig. S6.

We tested the predictions of this analysis by measuring the tube radii as described above and then using Eqs. **4** and **5** to compute the fluid flow at each point in the tube. Fig. 2*C* shows the predicted flows along the tube over time. To compare predictions and observations we measured the times of flow reversals in experiments, depicted in Fig. 2*C* by dashed lines. Theoretical predictions of the time points of flow reversals quantitatively agree with experiments. Although the flow dynamics agree, we find that the predicted velocities are significantly (10-fold) smaller than experimental measurements (Fig. S2). This is likely due to the measured outer radius of the tube being different from the inner radius, which actually drives the flow (28) and the exchange of matter between the fluid cytoplasm and the gel-like outer layer (29, 30).

Flows Are Controlled by Spatial Pattern of the Phase of Contractions. We next explored global patterns of flow across entire slime molds. The spatiotemporal development of a periodically contracting tube is shaped by four parameters: the spatial pattern of phase, the baseline radius of the tube, and the amplitude and period of the contractions (Fig. 1*B*). In principle, *P. polycephalum* could use any of these parameters to control flow patterns. A striking feature of observed networks is the reproducible arrangement of phases in a pattern, which appeared as the most likely control parameter in our experiments. By contrast, the tube radius and its distribution can vary widely from organism to organism, and tube radii grow and shrink as an organism forages for food or adapts to its environment. The timescale of morphological rearrangements (~45 min) is much larger than the timescale over which flow is generated (~100 s). The periods of contractions between different tube segments do not vary significantly over the whole organism or over time, at least not during the time course of our experiments of 1.5 h (average period ± SD is 131 ± 43 s for the organism in Fig. 3*A*). The amplitudes of contractions are somewhat correlated with the tube radii, with bigger tubes showing bigger contractions (Fig. S3). However, along a single tube, the amplitudes of contractions are variable, mostly because of fluctuations in the contractions (Fig. S4). However, the period and amplitude distributions are peaked (Fig. S5). For these reasons we focused our analysis on the phase of contraction as the primary parameter controlling global patterns of flow on timescales less than 1 h.

We documented the patterns of phases for organisms of different sizes, ranging from 3 to 17 mm. Results show a robust, reproducible behavior, and typical examples of a large-, a medium-, and a small-sized network are displayed in Fig. 3. Contractions cycle over time, and the phase of the contractions at any single point in an individual increases linearly as time passes (Fig. 3, *Top* to *Bottom*). However, the spatial phase gradient between adjacent points along a tube stays constant. The phase gradient is almost linear and the maximal spatial phase gradient over the whole organism equals a whole cycle of zero to 2π; strikingly, this pattern is irrespective of the organism size. In the framework of a peristaltic wave we observe that there is always about one wavelength encompassed within an organism of *P. polycephalum*. Furthermore, the orientation of the phase gradient in space stays roughly constant along the direction of the longest axis of the network in the case of spatially anisotropic organisms, whereas it can assume virtually any direction in the case of spatially isotropic organisms (Movies S2–S4). The slime mold *P. polycephalum* is known to grow to an arbitrary size, as long as food and the right environment are provided, which raises the question of the scale at which the adaption of the phase gradient to size breaks. We investigated organisms as large as 2.1 cm and still observed a single wavelength (Fig. S7). Our observations are consistent with previous research on the scaling of the Adenosine-5′-triphosphate gradient with organism size, observed up to sizes of 50 cm (31).

A Contraction Pattern Consisting of a Single Wavelength Across an Organism Optimizes Transport. To explore the transport properties conferred by *P. polycephalum*'s choice of phase pattern we built a theoretical description of the phase patterns in the network. Previous research proves a linear phase gradient is optimal for transporting matter down a tube when the mechanism of movement is peristalsis (14). However, the slime mold grows as

a random, closed network without net mass transport on the timescales considered in this work. Mass conservation imposes that the sum of contraction-driven flows ΔQ_j in all tubes $j \in N$ has to total zero,

$$\sum_{j \in \text{tubes}}^{N} \Delta Q_j = 0. \quad [6]$$

This has a profound effect on the allowed phase patterns in the network. To investigate, we neglect variations in the contraction period $2\pi/\omega$, amplitude ε, and base radius a_0 and consider cross-sectional contractions of the form

$$a^2(z,t) = a_0^2 + 2a_0\epsilon e^{i(\varphi-\omega t)}. \quad [7]$$

Eq. **5** then simplifies to

$$\Delta Q(z,t) = ia_0\epsilon 2\pi\omega e^{-i\omega t}\int_{z_0}^{z} dz' e^{i\varphi(z')}. \quad [8]$$

We assume that networks are discretized into segments of length ℓ, where the phase within each tube segment is approximately constant. This is a good approximation as long as the characteristic length scale of contractions is much larger than the tube segment size considered. If φ_j is the phase within the jth tube segment, conservation of mass in Eq. **6** implies

$$ia_0\epsilon 2\pi\omega\ell e^{-i\omega t}\sum_{j \in \text{tubes}}^{N} e^{i\varphi_j} = 0. \quad [9]$$

The general solution to this constraint is given by any integer partition of N, where the smallest addend is 2: Namely, if we consider any sum $\sum_k^K N_k = N$, with each $N_k \geq 2$, then the phases are given by

$$\varphi_{j(k)} = \frac{2\pi j}{N_k}. \quad [10]$$

For the spatial arrangement of the phases we choose a linear gradient, in which case any set partition with more than one element gives rise to multiple phase waves along the network. The solution with a single wavelength across the organism has the phases of the tubes being the Nth roots of unity; i.e., $\varphi_j = 2\pi j/N$, $j = 1,\ldots,N$. All of these solutions equally satisfy conservation of mass; the fact that *P. polycephalum* chooses a solution with a single wavelength per organism implies that there must be another constraint. We know from a single closed peristaltic tube that transport is maximized for a single wavelength, because particles do not need to travel past any node point, where the fluid flow vanishes (*SI Text*). In this simple scenario transport is optimized by a phase pattern going linearly from zero to 2π from one end of the vein to the other, which is equivalent to minimizing the overall phase difference.

Does this argument translate to a network of contracting tubes? To investigate this, we choose phases from a solution set in Eq. **10** with $N_k = N$ and then find the spatial distribution of phases that minimizes the local differences between the phases. We do this by first randomly distributing the phases and then using a Monte Carlo scheme that iterates possible spatial phase distributions by swapping phases between two tubes if favorable to achieve small phase differences throughout the network (*Materials and Methods*). Fig. 4, *Insets A* and *B*, show a random and an optimized phase pattern for the *P. polycephalum* network architecture mapped from the large organism in Fig. 3*A*, discretized into tube segments of length $\ell = 0.3274$ mm, at least an order of magnitude smaller than the extent of the organism L, *i*.e., the length scale of the phase pattern.

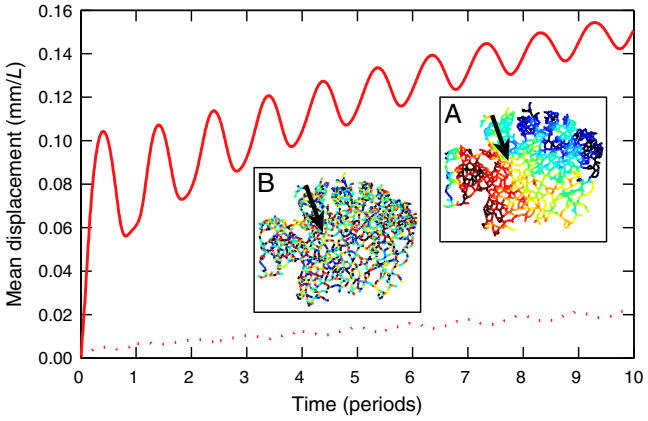

Fig. 4. Networks optimized for minimal local phase difference maximize particle transport. Numerically calculated mean displacement of tracer particles within the large real *P. polycephalum* network architecture of Fig. 3*A* is shown here for theoretically optimized (*Inset A*, solid line) and random (*Inset B*, dashed line) phase patterns. The mean displacement is normalized by the largest distance L in the network. Arrows mark the site of tracer initiation.

Given the phase patterns, we can now assess the transport properties of the corresponding networks. We compute for each homogeneously contracting tube segment the contractions from Eq. **7** and fluid flows generated by the contractions, using Eq. **4**. The flow boundary conditions for every single tube are calculated by imposing Kirchhoff's circuit law. We derive the Taylor dispersion for a contracting tube, which is used to equate the advection–dispersion of a cloud of tracer particles and to determine the mean distance the cloud travels within the network (*Materials and Methods*). Fig. 4 shows the displacement, normalized by the largest distance L within a network, of a particle cloud over 10 periods of contractions (Movies S5 and S6). The optimized phase pattern outperforms the random phase pattern more than sevenfold in spread after 10 periods and reaches more than 15% of the total distance within the network, whereas the random phase pattern covers only about 2%. In the network with the random phase pattern, particles essentially diffuse with the molecular diffusion constant κ on the scale of the tube segment, being mixed fast due to the oscillating flow within individual tube segments. With the long-ranged correlated phases in the optimized network the overall flow velocity is highly enhanced. When particles diffuse between faster and slower streamlines, the net diffusivity of particles is enhanced by a term $\overline{u}^2a^2/\kappa \sim \epsilon^2L^2\omega^2/\kappa$. By the nature of the shuttle flow, there is no selected orientation of transport, and particles are transported away from wherever they enter the network. However, the particle diffusivity is not isotropic, given that it is proportional to the squared flow velocity. Dispersal is, thus, fastest for particles halfway along the phase gradient, spreading uniformly either way along the direction of the gradient. This finding is similar to that of a single, closed peristaltic tube, now generalized to a random network.

Phase Patterns Optimized for Particle Transport Agree with *P. polycephalum* Patterns. To what degree are the phase patterns found in *P. polycephalum* peristaltic waves on a network? In a single peristaltic tube the signature of the spatial phase pattern is unmistakably reflected in the spatial phase correlation. The linear increase from zero to 2π gives rise to a cosine for the phase correlation, with perfect anticorrelation for phases separated by $L/2$ and perfect correlation for phases separated by L (Fig. 5*B*). To compare we now calculate the phase correlation for both

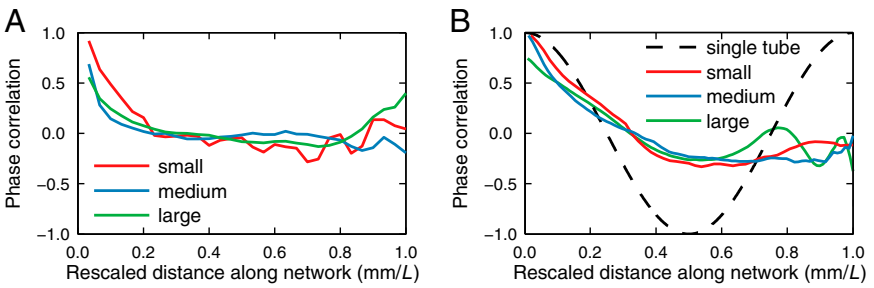

Fig. 5. (*A* and *B*) Qualitative agreement between measured (*A*) and theoretically derived (*B*) phase correlations for individuals shown in Fig. 3. All phase correlations display a single minimum, as predicted for a single wavelength along a tube shown in *B*. At large distances correlations are averaged out because much of the network extends perpendicular to the direction of the gradient. Experimental data are mean values averaged from a 276-s time frame; theoretical data are the mean of 100 independent runs, and so the statistical error is less than line thickness.

the experimentally measured phase patterns in *P. polycephalum* and the theoretically derived phase patterns on the observed *P. polycephalum* network architectures shown in Fig. 3. We define the phase correlation $c(x)$ by the sum over the dot products of the vector representation of any pair of phases in the network at a distance x,

$$c(x) = \frac{1}{2N}\sum_{k\in N}\left[\frac{1}{n_k(x)}\sum_{j\in V_k(x)}\vec{t}_k\vec{t}_j\right] \text{ with } \vec{t}_j = \begin{pmatrix}\cos\varphi_j\\ \sin\varphi_j\end{pmatrix}, \qquad [11]$$

with $V_k(x)$ the ensemble of tubes at a normalized distance x of tube k and $n_k(x)$ its cardinal. Both the experimental and the theoretical phase correlations displayed in Fig. 5 *A* and *B*, respectively, show a minimum for phases separated by $L/2$ and higher correlations for larger distances—the characteristics of a single wavelength stretching along the longest axis of the network. In the networks pairs of phases perpendicular to the direction of the phase gradient average out the correlations and anticorrelations relative to the case of a single peristaltic tube. On the small network the small number of tube segments lets fluctuation crumple up the phase correlation. For the theoretical phase patterns on the large network additional maxima and minima appear for large distances between phases due to the limitations of our very simple Monte Carlo procedure. Forcing the phase gradient along the shortest axis in a network in the simulations gives rise to a qualitatively very different phase correlation not observed in *P. polycephalum* (Fig. S8). Thus, the optimal phase gradient in a spatial anisotropic network forms along the longest axis of the network to maximize fluid flow and, hence, transport both in theory and in *P. polycephalum*.

Discussion

Cytoplasmic flows in networks of *P. polycephalum* organize on the scale of the whole organism and are caused by a generalized version of peristalsis. Our model suggests the movement of signals and substrates will be optimized when the wavelength of the peristaltic wave is of the order of the size of the network. Our data confirm these phase patterns are found within real individuals of *P. polycephalum*, independent of organism size. In fact, transport is optimized to the extent that the direction of the phase gradient in a network coincides with the longest axis of an anisotropic individual.

Transport is essential to share information and resources across an organism. For *P. polycephalum* Nakagaki et al. (19) found that environmental conditions can perturb the organism's contraction patterns, even giving rise to patterns with multiple wavelengths. They note that these multiple wavelengths manifest themselves with very slow solute dispersion, corroborating our finding that transport is optimal with a single wavelength, which is actively maintained by *P. polycephalum*.

How does an organism without a nervous system coordinate its growth and adapt flow to size, even specifically to the longest axis of an individual? In our theory the peristaltic wave patterns result from the interplay of a local rule (minimizing the phase differences between neighboring vein segments) and a global constraint (mass conservation). The global constraint may facilitate long-range interactions within any individual of arbitrary size: Although a local change in phase alters locally generated flow, because mass is conserved, it also alters flows and phases elsewhere, enabling dynamics at one part of the network to influence dynamics across an individual. The constraint also explains the lack of any local correlation between contractions and fluid flows at any single point of the network, an observation that led to the dismissal of peristalsis as a mechanism of transport in previous works (22–25).

Flows may enable the movement of resources within an individual and avoidance of repellents. Attractive stimuli, including food sources, increase the frequency of contractions, whereas repellents decrease the frequency of contractions (32). In the context of peristaltic waves, the difference implies that attractants internalized into a network of veins will spread faster than repellents. If food or toxins are encountered at the rim of a network, a gradient in the amount of the substance distributed across the network will persist for a long time, because flow velocity and thus transport vanish at vein ends. Because the food source or toxin will not be homogenized throughout the network, the organism may be able to use the gradient to "remember" and find or avoid the location of the food source or toxin. These dynamics may also explain an aspect of the natural history of *P. polycephalum*. A foraging individual quickly reforms its center around a food source, for example an oat flake, perhaps because resources will be more efficiently distributed when they are not at the edges of a network.

We provide a quantitative model of fluid flows within a slime mold, enabling a mechanistic understanding of *P. polycephalum*'s behaviors; the concepts may translate to other organisms growing as networks and particularly to fungi. Striking morphological and behavioral similarities (33), and the discovery of oscillatory nutrient transport within basidiomycetes (34), suggest common mechanisms. Knowledge of the flow dynamics within fungal individuals is limited, but the global constraint of mass conservation will hold for fungal networks. Internal flows may also function to coordinate behaviors among the fungi, a kingdom with critical relevance for ecosystems.

Materials and Methods

Preparation and Imaging of *P. polycephalum*. Plasmodia of *P. polycephalum* (Carolina Biological Supplies) were grown on 1.5% (wt/vol) agar without nutrients and fed daily with oat flakes (Quaker Oats Company). Eight to 24 h before imaging, either a newly colonized oat flake or the tip of a foraging plasmodium was transferred to a new Petri dish. Results from oat flake plasmodia and growing tips were indistinguishable. Slime molds were modified by removing growing fans and imaged by transmitted light microscopy, using a Zeiss Lumar.V12 stereomicroscope, at magnifications between 1.0× and 10.0×. Petri dishes were illuminated from below, using white light-emitting diodes on a transmitted light stage (Schott TLS-BF; 84 mm). A long-pass filter with cutoff $\lambda = 610$ nm (20CGA-610; Newport) and a plastic light diffuser were placed on top of the light stage. Light intensities were controlled with a custom-made Matlab code (The Mathworks). Images were taken every 6 s.

Simulating Phase Patterns of Minimal Phase Difference. We simulated spatial phase patterns of minimal phase difference with a Metropolis Monte Carlo simulation, using a custom-written Matlab program (The Mathworks). Phases satisfying conservation of mass, as stated in Eq. **10**, were initially randomly distributed over the tubes and subsequently the total sum of the squared phase differences at every node was minimized,

$$E = \sum_{j \in \text{tubes}} \sum_{k \in \mathcal{C}(j)} (\varphi_j - \varphi_k)^2, \qquad [12]$$

where $\mathcal{C}(j)$ denotes all tubes that are immediate neighbors of tube j. To minimize phase differences two randomly chosen phases were interchanged according to the Metropolis Monte Carlo procedure. For a large system size N, where n = number of tube segments, initially aligning the phases linearly according to the distance between two chosen fixed endpoints bearing the smallest and the largest phase, respectively, facilitated the path to a local minimum. In detail, every tube was scored according to its value of $D = d_s + N - d_e$, where d_s and d_e denote the minimal distance along the network to the start and the end tubes, respectively. Then, the phases were distributed from the smallest value at the start tube to the largest value at the end tube according to values of D. We randomly distributed phases within the class of equivalent Ds. We chose endpoints randomly within a boundary layer of a sector close to the largest axis of the network's enclosing ellipse unless stated otherwise.

Simulating Contraction-Driven Flow in a Closed Network of Tubes. A customized Matlab program (The Mathworks) was written to solve for the flows generated by a network of contracting tubes. Given a specific spatial pattern of phases, the accompanying cross-sectional contractions and fluid flows arising from contractions are calculated according to Eqs. **4**, **5**, and **7**, assuming parameter values of $a_0 = 50$ μm, $\epsilon = 0.1 a_0$, and $\omega = 0.05$ Hz. The additional flow component caused by inflows from neighboring tubes is computed by imposing Kirchoff's circuit law. Toward this end, the flows arising only from contractions in individual tubes were interpreted as inflows at network nodes, and then the additional flow component at every time step was derived as in ref. 8.

The advection–dispersion of the cross-sectionally averaged concentration of tracer particles $\overline{C}$ within the flow was simulated with a Crank–Nicolson implementation of a partial differential equation describing the effective transport dynamics along the longitudinal axis, also known as Taylor dispersion (35, 36). The Taylor dispersion in a contracting tube was derived with the center manifold approach introduced by Mercer and Roberts (37) and was eventually found to be equivalent to the dispersion in a rigid tube with spatially varying cross-section (38),

$$\frac{\partial \overline{C}}{\partial t} = \frac{\partial}{\partial z}\left\{\left(-\overline{u} - \frac{\overline{u}^2 a}{24\kappa}\frac{\partial a}{\partial z} + 2\frac{\kappa}{a}\frac{\partial a}{\partial z}\right)\overline{C} + \left(\kappa + \frac{\overline{u}^2 a^2}{48\kappa}\right)\frac{\partial \overline{C}}{\partial z}\right\}, \qquad [13]$$

where κ denotes the molecular diffusivity.

ACKNOWLEDGMENTS. We thank Jacques Dumais for early support and Natalie Andrew for assistance. This research was funded by the Human Frontiers Science Program, the National Science Foundation through the Harvard Materials Research Science and Engineering Center (DMR-0820484), the National Institutes of Health National Institute of General Medical Sciences Grant GM068763 for National Centers of Systems Biology, and the Deutsche Akademie der Naturforscher Leopoldina (K.A.) and Ministére de l'Economie et des Finances - Corps des Mines (F.P.). M.P.B. is an Investigator of the Simons Foundation.

1. Boddy L, Hynes J, Bebber DP, Fricker MD (2009) Saprotrophic cord systems: Dispersal mechanisms in space and time. *Mycoscience* 50(1):9–19.
2. Nakagaki T, Guy R (2008) Intelligent behaviors of amoeboid movement based on complex dynamics of soft matter. *Soft Matter* 4(1):57–67.
3. Nakagaki T, et al. (2007) Minimum-risk path finding by an adaptive amoebal network. *Phys Rev Lett* 99(6):068104.
4. Nakagaki T, Yamada H, Tóth A (2000) Maze-solving by an amoeboid organism. *Nature* 407(6803):470.
5. Tero A, et al. (2010) Rules for biologically inspired adaptive network design. *Science* 327(5964):439–442.
6. Dussutour A, Latty T, Beekman M, Simpson SJ (2010) Amoeboid organism solves complex nutritional challenges. *Proc Natl Acad Sci USA* 107(10):4607–4611.
7. Durand M (2007) Structure of optimal transport networks subject to a global constraint. *Phys Rev Lett* 98(8):088701.
8. Corson F (2010) Fluctuations and redundancy in optimal transport networks. *Phys Rev Lett* 104(4):048703.
9. Katifori E, Szöllosi GJ, Magnasco MO (2010) Damage and fluctuations induce loops in optimal transport networks. *Phys Rev Lett* 104(4):048704.
10. Kamiya N (1950) The rate of the protoplasmic flow in the myxomycete plasmodium I. *Cytologia* 15(3-4):183–193.
11. Stewart PA, Stewart BT (1959) Protoplasmic movement in slime mold plasmodia; the diffusion drag force hypothesis. *Exp Cell Res* 17(1):44–58.
12. Isenberg G, Wohlfarth-Bottermann KE (1976) Transformation of cytoplasmic actin. Importance for the organization of the contractile gel reticulum and the contraction—relasation cycle of cytoplasmic actomyosin. *Cell Tissue Res* 173(4):495–528.
13. Carew EOPTJ, Pedley TJ (1997) An active membrane model for peristaltic pumping: Part I—Periodic activation waves in an infinite tube. *J Biomech Eng* 119(1):66–76.
14. Shapiro A, Jaffrin M, Weinberg S (1969) Peristaltic pumping with long wavelengths at low Reynolds number. *J Fluid Mech* 37:799–825.
15. Seifriz W (1953) Mechanism of protoplasmic movement. *Nature* 171(4365):1136–1138.
16. Stewart PA (1964) The organization of movement in slime mold plasmodia. *Primitive Motile Systems in Cell Biology*, ed Aleen R (Academic, New York).
17. Iima M, Nakagaki T (2012) Peristaltic transport and mixing of cytosol through the whole body of *Physarum* plasmodium. *Math Med Biol* 29(3):263–281.
18. Matsumoto K, Ueda T, Kobatake Y (1988) Reversal of thermotaxis with oscillatory stimulation in the plasmodium of *Physarum polycephalum*. *J Theor Biol* 131(2): 175–182.
19. Nakagaki T, Yamada H, Ueda T (2000) Interaction between cell shape and contraction pattern in the *Physarum* plasmodium. *Biophys Chem* 84(3):195–204.
20. Ueda T (2005) An intelligent slime mold: A self-organizing system of cell shape and information. *World Scientific Lecture Notes in Complex Systems: Network of Interacting Machines*, eds Armbruster D, Kaneko K, Mikhailov AS (World Scientific, Singapore): 221–256.
21. Takagi S, Ueda T (2008) Emergence and transitions of dynamic patterns of thickness oscillation of the plasmodium of the true slime mold *Physarum polycephalum*. *Physica D* 237:420–427.
22. Achenbach U, Wohlfarth-Bottermann K (1981) Synchronization and signal transmission in protoplasmic strands of *Physarum*. *Planta* 151:584–594.
23. Grebecki A, Cieślawska M (1978) Plasmodium of *Physarum polycephalum* as a synchronous contractile system. *Cytobiologie* 17(2):335–342.
24. Samans K, Hinz I, Hejnowicz Z, Wohlfarth-Bottermann K (1984) Phase relation of oscillatory contraction cycles in *Physarum* plasmodia: I. A serial infrared registration device and its application to different plasmodial stages. *J Interdiscipl Cycle Res* 15: 241–250.
25. Hejnowicz Z, Hinz I, Wohlfarth-Bottermann KE (1984) Phase relations of oscillatory contraction cycles in *Physarum* plasmodia: II. Occurrence of type 0 resetting. *J Interdiscipl Cycle Res* 15:251–266.
26. Uchida S, Aoki H (1977) Unsteady flows in a semi-infinite contracting or expanding pipe. *J Fluid Mech* 82:371–387.
27. Secomb T (1978) Flow in a channel with pulsating walls. *J Fluid Mech* 88:273–288.
28. Grebecki A, Cieslawska M (1978) Dynamics of the ectoplasmic walls during pulsation of plasmodial veins of *Physarum polycephalum*. *Protoplasma* 97:365–371.
29. Hülsmann N, Wohlfarth-Bottermann KE (1978) Räumliche und zeitliche Analyse von kontraktionsabhängigen Oberflächenbewegungen bei *Physarum polycephalum* [Spatio-temporal analysis of contraction dependent surface movements in *Physarum polycephalum*]. *Cytobiologie* 17(1):23–41.
30. Hülsmann N, Wohlfarth-Bottermann KE (1978) Spatio-temporal relationships between protoplasmic streaming and contraction activities in plasmodial veins of *Physarum polycephalum*. *Cytobiologie* 17(2):317–334.
31. Ueda T, Mori Y, Kobatake Y (1987) Patterns in the distribution of intracellular ATP concentration in relation to coordination of amoeboid cell behavior in *Physarum polycephalum*. *Exp Cell Res* 169(1):191–201.
32. Ueda T, Muratsugu M, Kurihara K, Kobatake Y (1976) Chemotaxis in Physarum polycephalum. Effects of chemicals on isometric tension of the plasmodial strand in relation to chemotactic movement. *Exp Cell Res* 100(2):337–344.
33. Fricker M, Boddy L, Nakagaki T, Bebber D (2009) Adaptive biological networks. *Adaptive Networks*, Understanding Complex Systems (Springer, Berlin), eds Gross T, Sayama H, pp 51–70.
34. Fricker MD, et al. (2008) Imaging complex nutrient dynamics in mycelial networks. *J Microsc* 231(2):317–331.
35. Taylor G (1953) Dispersion of soluble matter in solvent flowing slowly through a tube. *Proc R Soc A* 219(1137):186–203.
36. Aris R (1956) On the dispersion of a solute in a fluid flowing through a tube. *Proc R Soc A* 235(1200):67–77.
37. Mercer GN, Roberts AJ (1990) A center manifold description of contaminant dispersion in channels with varying flow properties. *SIAM J Appl Math* 50:1547–1565.
38. Mercer GN, Roberts AJ (1994) A complete model of shear dispersion in pipes. *Japan J Indust Appl Math* 11:499–521.

Supporting Information

Alim et al. 10.1073/pnas.1305049110

SI Text

Particle Transport in a Closed Peristaltic Tube Is Maximal for a Single Wavelength. To show that a single wavelength maximizes transport we calculate the maximal distance traveled by a particle in a single closed tube of length L. We impose a peristaltic wave satisfying conservation of mass by choosing a linear phase gradient defined by $\varphi(z) = 2\pi nz/L$. As long as n is an integer, mass is conserved. Now we can solve for a particle's trajectory along the center line of the tube by equating $dz(t)/dt = 2\overline{u}(z,t)$, using the contractions defined in Eq. **7**. For small contraction amplitudes ε, the maximal distance traveled by a particle starting at position z_0 is

$$\Delta z_{\max} = \frac{4\epsilon L}{a_0 n\pi}(1-\cos(2n\pi z_0/L))|\sin(\pi n z_0/L)|. \qquad \textbf{[S1]}$$

Hence, the distance a particle travels is maximized for $n = 1$, i.e., for a single wavelength, because the particle does not need to pass by any node points, where the fluid flow is zero.

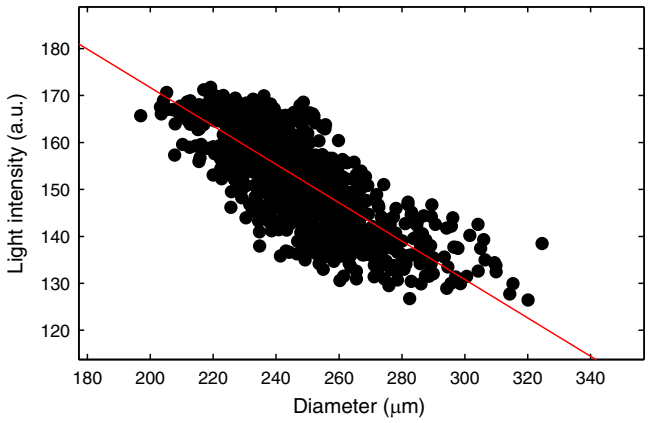

Fig. S1. Correlation between the transmitted light intensity through a vein and the diameter of the vein.

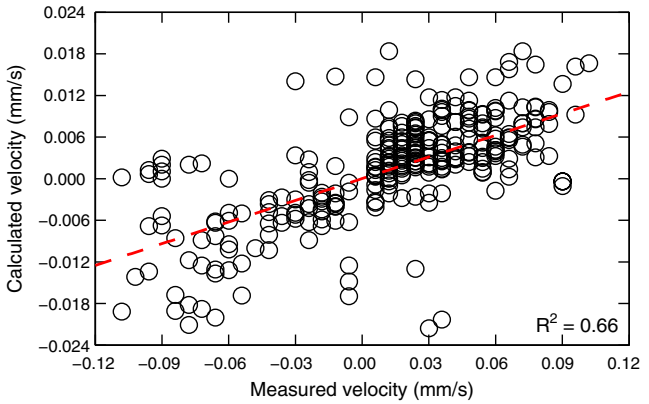

Fig. S2. Quantitative comparison of experimentally measured velocities and velocities calculated from the contracting vein model based on measured vein radii. The calculated velocities are a factor of 10 smaller than measured velocities. This is likely due to the measured outer radius of the tube being different from the inner radius, which actually drives the flow and the exchange of matter between the fluid cytoplasm and the gel-like outer layer.

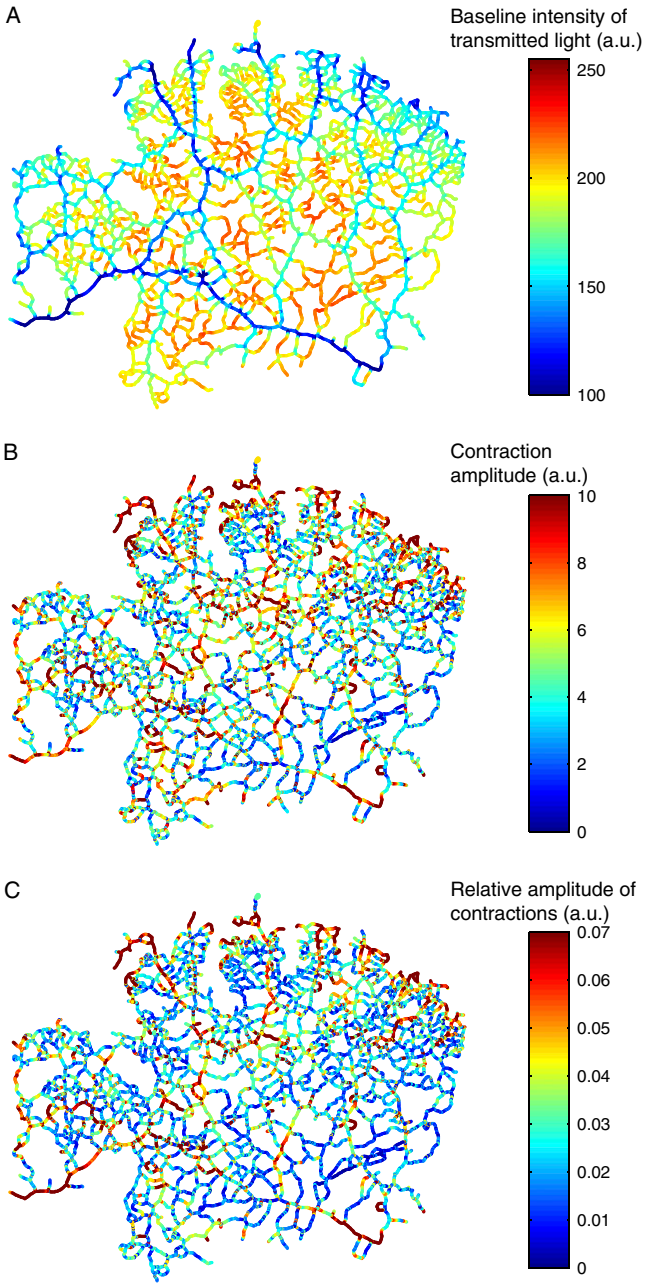

Fig. S3. Spatial pattern of contraction amplitudes for the large slime mold shown in in Fig. 3*A*. (*A*) Baseline intensity (inversely correlated to the vein radius). (*B*) Contraction amplitude. (*C*) Relative amplitude of the contractions, defined as the ratio between the amplitude of contractions in light intensity and the average transmitted light intensity through the vein (sliding average over 10 min).

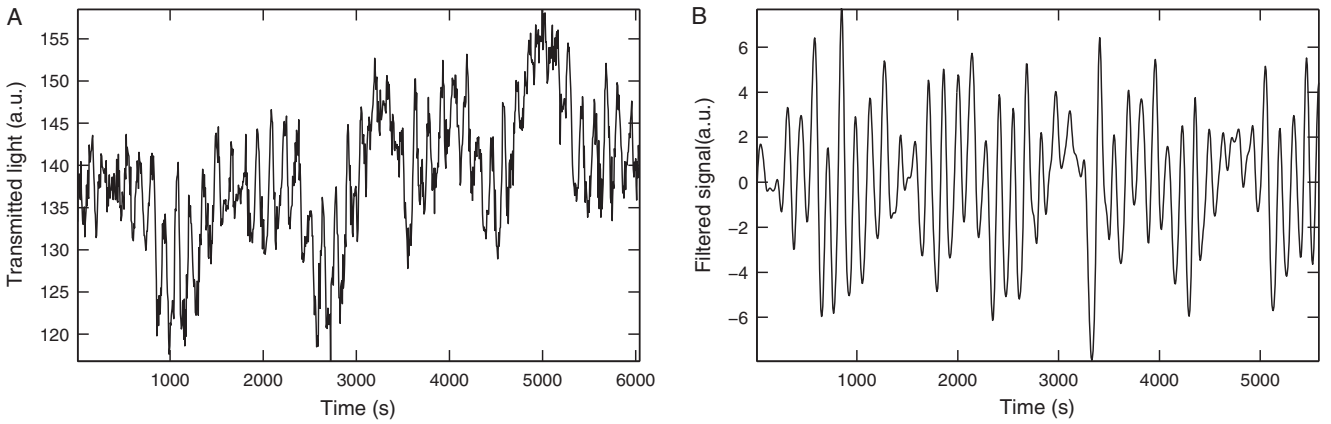

Fig. S4. Variability of contraction amplitudes. (*A*) A typical time series of transmitted light intensity through a vein. (*B*) The same time series as in *A*, detrended by subtracting the local mean (running average over 10 min) and filtered with a Gaussian filter of width $\sigma = 18s$. These are the data that are used in all further data analysis (determining the phase of the contractions, their amplitude, and period).

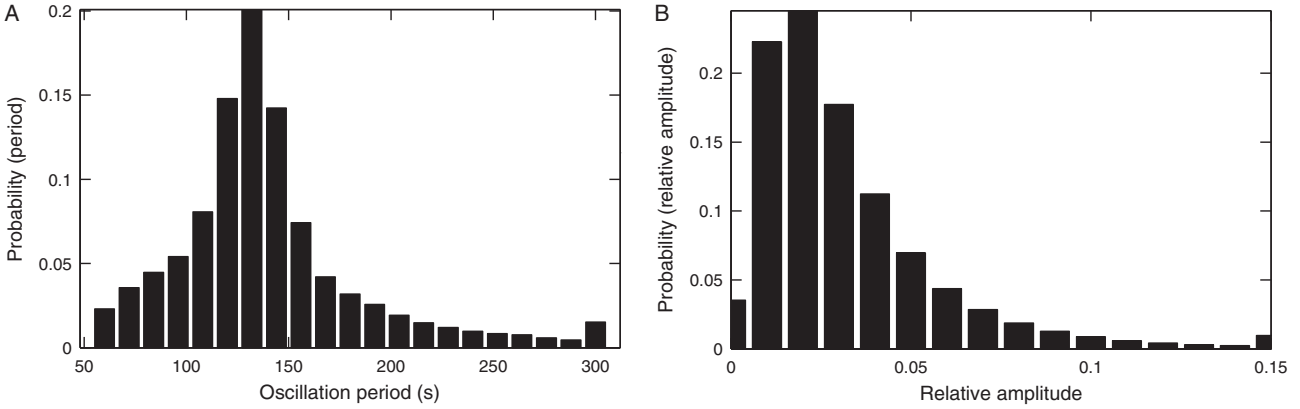

Fig. S5. Distribution of contraction parameters for all veins of the large slime mold shown in Fig. 3*A*. (*A*) Histogram of the period of contractions. (*B*) Histogram of the relative amplitude of the oscillations in transmitted light intensity. The relative amplitude of oscillations is defined as the ratio between the amplitude of oscillations in light intensity and the average transmitted light intensity through the vein (sliding average over 10 min).

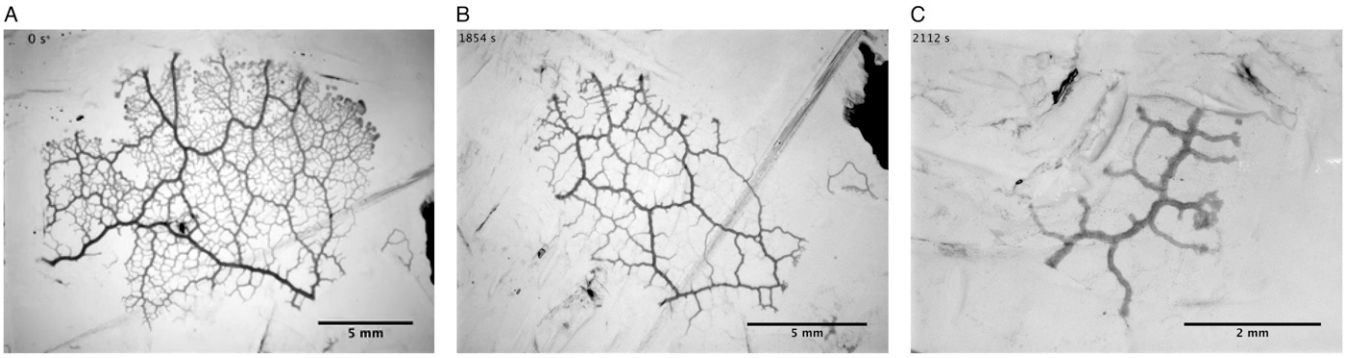

Fig. S6. (*A–C*) Bright-field microscopy snapshot of the (*A*) large, (*B*) medium, and (*C*) small *P. polycephalum* networks of Fig. 3.

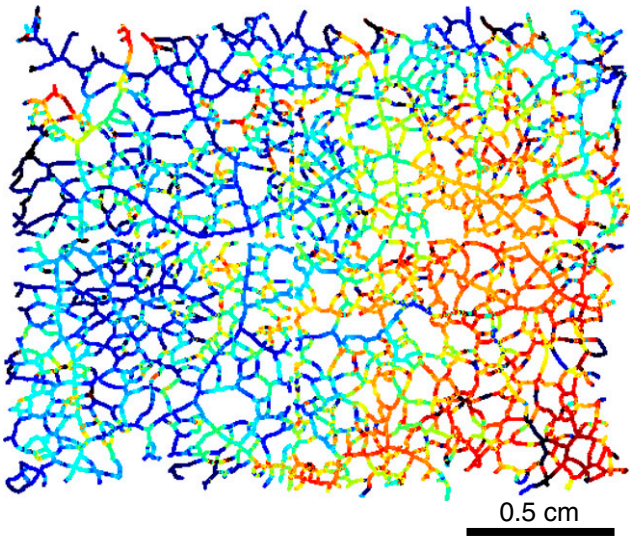

Fig. S7. Phase pattern within the largest network of *P. polycephalum* analyzed by us, extending up to 2.1 cm.

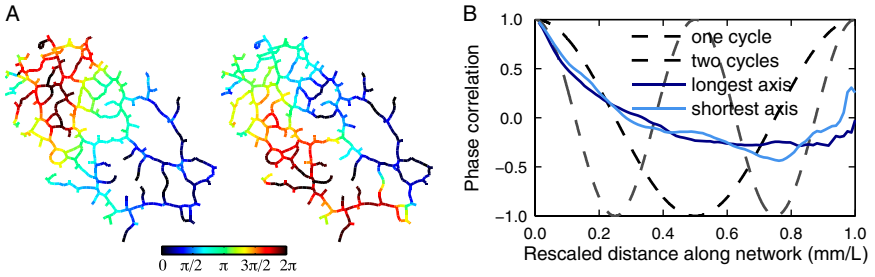

Fig. S8. Comparison of phase gradient aligned along the longest and the shortest spatial extent. (*A*) Phase pattern forced along the longest and shortest spatial extents by keeping the smallest and the largest phase fixed at opposing vein segments in the spatially anisotropic *P. polycephalum* network architecture of Fig. 3*B*. (*B*) Phase correlation displays two minima for the phase gradient along the shortest axis in comparison with the single minimum for the phase gradient along the longest axis, turning the orientation of the phase gradient distinguishable within the phase correlation.

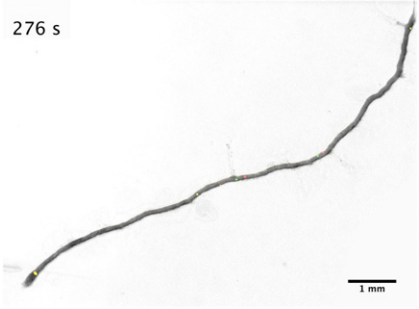

Movie S1. Fluorescent beads of diameter 1 μm were endocytosed by *P. polycephalum* and tracked. Red and green dots correspond to the positions of the beads at 1-s intervals.

Movie S1

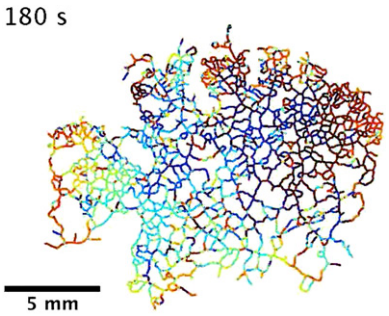

Movie S2. Evolution of phase pattern of the large slime mold individual of Fig. 3*A* over time. The color code indicates the phase of the contractions as the fraction of the contraction elapsed relative to the last maximum. The color code is periodic, cycling from black at zero to blue, green, and red and back to black at a phase of 2π.

Movie S2

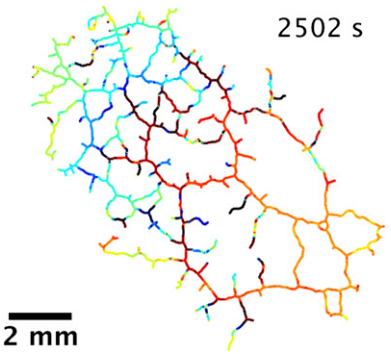

Movie S3. Evolution of phase pattern of the medium slime mold individual of Fig. 3*B* over time. The color code indicates the phase of the contractions as the fraction of the contraction elapsed relative to the last maximum. The color code is periodic, cycling from black at zero to blue, green, and red and back to black at a phase of 2π.

Movie S3

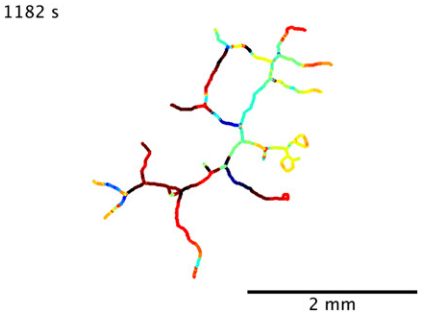

Movie S4. Evolution of phase pattern of the small slime mold individual of Fig. 3*C* over time. The color code indicates the phase of the contractions as the fraction of the contraction elapsed relative to the last maximum. The color code is periodic, cycling from black at zero to blue, green, and red and back to black at a phase of 2π.

Movie S4

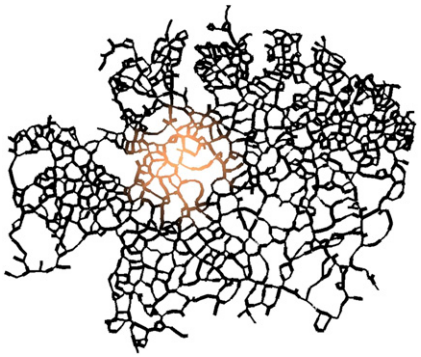

Movie S5. Concentration profile of a cloud of tracer particles dispersion over 10 periods within the large *P. polycephalum* network architecture of Fig. 3*A* for random phases. Corresponding phase pattern is shown in Fig. 4, *Inset B*. Radii of vein segments scale with the actual contraction state of the vein. Logarithmic scale for concentration profile goes from high (bright) to zero (black).

Movie S5

Movie S6. Concentration profile of a cloud of tracer particles dispersion over 10 periods within the *P. polycephalum* network architecture of Fig. 3*A* for optimized phases. Corresponding phase pattern is shown in Fig. 4, *Inset A*. Radii of vein segments scale with the actual contraction state of the vein. Logarithmic scale for concentration profile goes from high (bright) to zero (black).

Movie S6